Pergamon

Int. J. Solids Structures Vol. 35, No. 14, pp. 1653–1675, 1998

0020-7683/98 $19.00 + .00

PII: S0020-7683(97)00129-7

ANALYSIS OF OUT-OF-PLANE BENDING IN ONE-SIDED BONDED REPAIR

C. H. WANG, L. R. F. ROSE and R. CALLINAN
Aeronautical and Maritime Research Laboratory, Airframes and Engines Division, Defence Science and Technology Organisation, P.O. Box 4331, Melbourne, VIC 3001, Australia
E-mail: wang@aedmel.arl.dsto.gov.au

(*Received* 1 *October* 1996; *in revised form* 1 *May* 1997)

Abstract—An un-supported cracked plate repaired with a reinforcement bonded on one side may experience a considerable out-of-plane bending, resulting mainly from the load-path eccentricity. A geometrically linear analysis is presented in this paper for the crack extension force after the application of a one-sided repair. It is found that although the stress intensity factor K for a one-sided repair is higher than in two-sided repairs where there is no bending present, the key feature is retained that K does not increase indefinitely with increasing crack length, but instead approaches asymptotically a finite upper-bound corresponding to the solution for a semi-infinite crack. An analytical expression is derived for this upper bound, which provides a conservative estimate suitable for design purposes and parametric studies. This analytical solution is shown to agree well with a fully three-dimensional finite element analysis. Strategies to minimize the detrimental effect of out-of-plane bending are briefly discussed. © 1998 Elsevier Science Ltd.

NOMENCLATURE

a	crack length
D	bending stiffness ($=Et^3/12$)
E	Young's modulus
G	strain energy release rate
I	moment of inertia per unit width ($=t^3/12$)
k	spring constant for two sided repair
K_∞	upper pound stress intensity factor for two-sided repair
L	width of a finite plate
N	direct force in plate
M	bending moment
R	ratio between minimum and maximum stresses in a plate under combined tension and bending
S	stiffness ratio ($=E'_R t_R/E'_P t_P$)
t	thickness
U_E	elastic strain energy
x, y	in-plane coordinate
z	through-thickness coordinate
β	shear stress transfer parameter ($=\sqrt{(\mu_A/t_A)(1/E'_P t_P + 1/E'_R t_R)}$).
β_s	shear stress transfer parameter for single strap joint ($=2\beta$)
μ_A	adhesive shear modulus
ν	Poisson's ratio
ω	bending correction factor for one-sided repair
σ^∞	remote applied stress
σ_0	perspective membrane stress across crack front
σ_b	perspective bending stress across crack front
Π	potential energy

Subscripts

A	adhesive layer
P	cracked plate
R	reinforcement
rms	root-mean-square value
∞	parameters pertaining to semi-infinite crack

Superscripts

*	parameters pertaining to one-sided repair
′	Young's modulus under plane strain conditions

1. INTRODUCTION

The last two decades have witnessed significant advances in bonded repair technology as an efficient and cost-effective means of repairing cracks, especially in aircraft structures (Ratwani, 1979; Rose, 1981; Baker and Jones, 1988; Baker, 1993; Rose *et al.*, 1995). From a geometrical consideration, bonded repairs as illustrated in Fig. 1 fall into two categories: two-sided (symmetric) and one-sided (asymmetric). In the former case two identical reinforcements are bonded on the two surfaces of a cracked plate. This symmetric arrangement ensures that there is no out-of-plane bending over the repaired region, see Fig. 1(b), provided the cracked plate is subjected to extensional loads only. From a practical application viewpoint, the most important feature of (symmetric) bonded repairs is probably the asymptotic behaviour of the crack extension force as crack length increases. This means that the stress intensity factor after the repair approaches asymptotically, but never exceeds an upper bound, which depends on the geometry and material properties of a particular repair. The reason for this asymptotic behaviour is essentially due to that the repair provides a crack-bridging mechanism, such that the applied load can be fully transmitted across the crack with only a finite relative displacement between the crack faces, and this in turn ensures that the strain energy release rate for a semi-infinite crack is finite.

In actual repairs, however, one-sided repair is often adopted in which composite patches are applied to only one side of the panel (Baker and Jones, 1988; Baker, 1993; Rose *et al.*, 1995). This is because most often, only one face of a structure to be repaired is accessible and sometimes only one side of a structure is allowed to be patched, e.g. aircraft fuselage or wing sections. Provided the structure to be repaired is well supported against out-of-plane deflection, the analytical procedure developed by Rose (1981, 1987, 1988) has been shown to agree well with finite element results. However, in the case of unsupported one-sided repair, the out-of-plane bending caused by the shift of the neutral plane away from that of the plate may considerably lower the repair efficiency, as recognized by a number of authors in the literature (Ratwani, 1979; Jones, 1983; Rose, 1988; Arendt and Sun, 1994). In this regard, a recent finite element analysis by Arendt and Sun (1994) cast some serious doubt over the validity of the existing bonded repair methodology, as their results appeared to suggest that the stress intensity factor for a one-sided repair would increase indefinitely with increase crack length. Furthermore, this alarming result seems to agree with an earlier work by Ratwani (1979), who contended that the influence of bending

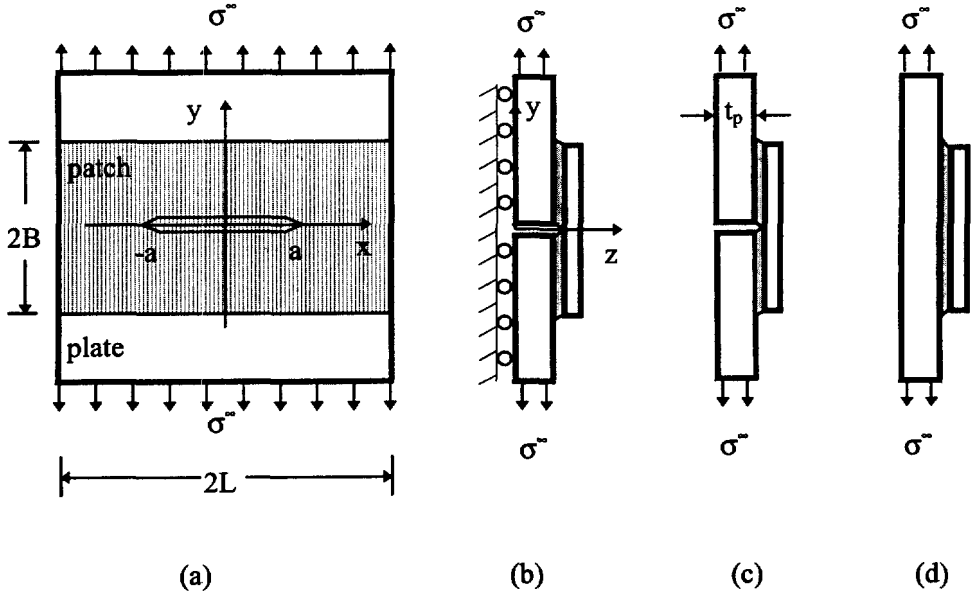

Fig. 1. Repair configurations and coordinates: (a) plan view; (b) cross-section along centre line ($x = 0$) with no bending deflection allowed, representing two-sided repair; (c) cross-section of a one-sided repair along the centre line; and (d) cross-section at $x \to \infty$ for a one-sided repair.

(increase in stress intensity factor) in a structure will increase indefinitely as the crack length increases.

The aim of this paper is to present a theoretical and numerical analysis of one-sided repairs, taking into account the out-of-plane bending effect. For the sake of simplicity, only a geometrically linear analysis is considered in this paper; the effect of geometrically non-linear deformation will be the subject of a separate paper. To quantify the effect of out-of-plane bending, an extensive finite element analysis has been carried out to verify the analytical solution. The most important finding is that the stress intensity factor of a one-sided repaired crack does asymptote to, but never exceeds, a limiting value, and that the analytical solution provides a *conservative* estimate for this limiting value.

2. REVIEW OF PREVIOUS WORK

For an isotropic centre-cracked panel of thickness $2t_P$ and Young's modulus of E_P, the asymptotic stress intensity factor after repair by a quasi-isotropic patch of thickness t_R and Young's modulus of E_R can be expressed as (Rose, 1982)

$$K_\infty = \sigma_0/\sqrt{k}, \tag{1}$$

where the subscript ∞ refers to the stress intensity factor of a repaired semi-infinite crack, σ_0 denotes the stress that would exist in an uncracked plate after the application of a patch, and k represents a spring constant given by eqn (3). For the case of strip-like patch as indicated in Fig. 1(a),

$$\sigma_0 = \frac{1}{1+S}\sigma^\infty, \tag{2}$$

where $S = E'_R t_R/E'_P t_P$. Here E'_R and E'_P represent, respectively, the Young's modulus of the plate and reinforcement under plane strain condition. The spring constant k in eqn (1) is given by (Wang and Rose, 1997a):

$$k = \frac{\beta S}{(1+S)(1-\nu_P^2)} \tag{3}$$

where β^{-1} is a shear stress transfer length in a representative bonded joint,

$$\beta = \left[\frac{\mu_A}{t_A}\left(\frac{1}{E'_P t_P} + \frac{1}{E'_R t_R}\right)\right]^{1/2}. \tag{4}$$

Here μ_A and t_A represent the shear modulus and the thickness of the adhesive layer. It should be pointed out that the spring constant given by eqn (3) has been derived by treating the represented bonded joint as under plane strain condition (Wang and Rose, 1997a), hence differs from that derived by Rose (1988), where the represented joint was assumed to be in plane stress.

In the case of one-sided repairs, Ratwani (1979) provided a bending correction factor for one-sided repairs based on the following considerations: (i) the stresses in the cracked plate and the reinforcement far away from the crack were assumed to be equal; (ii) the out-of-plane bending in a one-sided repair was entirely due to the presence of a crack. Postulating a relation

$$K^* = (1+BC)K_P, \tag{5}$$

where K_p refers to the stress intensity factor for a symmetric repair, and K^* the stress

intensity factor for a one-sided repair, the correction term BC is given by Ratwani (1979) as

$$BC = \left(1 - \frac{K_P}{K}\right) \frac{t_P(t_P + t_R) y_{max}}{I} a, \tag{6}$$

where K represents the stress intensity factor of the unrepaired crack, y_{max} signifies the distance of the extreme fibres of the cracked plate from the neutral axis of the cracked plate (i.e. $y_{max} = t_P/2$), and I is the moment of inertia of the plate, which is equal to $Lt_P^3/12$. Here, L denotes the width of the panel. A feature of this analysis as indicated by eqn (6) is that the bending correction factor increases linearly with crack length a. Furthermore, the result also predicted that the bending effect is negligible for crack lengths much smaller than panel width. Jones (1983, 1988) in a subsequent study adopted Ratwani's definition of BC, but noted from his numerical results that the influence of bending did not increase indefinitely, contrary to that suggested by Ratwani (1979). The reason for these conflicting results was not clarified, but it is believed by the present authors that Jones might have taken a different, inconsistent interpretation of the moment of inertia I from the original Ratwani's analysis. Nevertheless, the limited finite element results obtained by Jones (1983) supported the view that the stress intensity factor for one-sided repairs should remain bounded.

Of the two key assumptions made by Ratwani (1979), it should be noted first that the deformation in the plate and the reinforcement far away from the crack will be incompatible if the stresses are assumed to be the same, unless the extensional moduli of both the patch and the plate happen to be the same, which is not usually the case for composite bonded repairs to metallic (aluminium) structures. Secondly, probably more importantly, the out-of-plane bending in a one-sided repair, as will be demonstrated later, is induced by the shift of the neutral plane away from the mid-surface of the plate, rather by the loss of load-bearing cross-section due to the crack, as conjectured by Ratwani.

Rose (1988) correctly identified the existence of an asymptotic upper bound and the length scales induced by secondary bending. However, a constant term was overlooked in the governing equation for out-of-plane deflection. This oversight is corrected in the present work, within the framework of a geometrically linear analysis. It is thus clear from the previous discussion that the issue of one-sided repair remains unresolved; reports in the literature are often conflicting and contradictory. This has greatly hampered the design and analysis of one-sided bonded repairs, a case frequently encountered in repairing thin skin components, such as aircraft structures.

3. PROBLEM FORMULATION

Referring to Fig. 1, the problem being considered is that of a centre-cracked plate, with crack length $2a$, repaired by a bonded reinforcement in the form of a strip of height $2B$, running across the full width $2L$. A remote uniform tensile stress σ^∞ is applied to the plate normal to the crack. The problem is to determine the stress intensity factor K in the repaired plate, as a function of crack length $2a$ and of the relevant parameters pertaining to the patched system, notably the Young's modulus E and thickness t. Here, and in the following subscripts, P, R, A will be used to distinguish properties pertaining, respectively, to the plate, the reinforcement and the adhesive layer.

Due to the bending moment present in the repaired region, the stress, strain and displacement vary through the thickness of the plate, and consequently the stress intensity factor will also vary across the crack front. Within the framework of the shear deformation theory by Reissner (1947) for plates, the crack tip singular field for a cracked plate subjected to membrane and bending stresses has the same functional form as a plate under extensional load only [see Hartranft and Sih (1968); Sih (1971)], with the stress intensity factor varying linearly through the plate thickness. This means that the y-stress at position r ahead the crack tip can be expressed as:

$$\sigma_{yy}(r, y=0, z) = \frac{K(z)}{\sqrt{2\pi r}}. \tag{7a}$$

Similarly the near-tip crack opening displacement follows the standard asymptotic relation:

$$u_y(x \to a^-, y = 0^+, z) = \frac{4K(z)}{E}\sqrt{\frac{a-x}{2\pi}}, \tag{7b}$$

where $K(z)$ represents the stress intensity factor as a function of the through-thickness coordinate z.

Assuming a linear variation for $K(z)$, in accordance with shear deformation plate theories,

$$K(z) = K_{\text{mean}} + K_b \frac{2z}{t_P}, \tag{8}$$

where K_{mean} and K_b denote, respectively, the membrane and bending stress intensity factors. The total energy release rate, $t_P G$, across the thickness for self-similar crack growth is the energy released during a virtual crack extension of δa, which in turn is equal to the work done by hypothetically imposed surface tractions:

$$\begin{aligned} t_P G &= \lim_{\delta \to 0} \frac{\delta U_E}{\delta} = \lim_{\delta \to 0} \frac{1}{\delta} \int_0^{t_P} 2 \int_0^{\delta} \frac{\sigma_{yy}(r, z) u_y(\delta - r, z)}{2} \, dr \, dz \\ &= \lim_{\delta \to 0} \int_0^{t_P} \frac{2K^2(z)}{\pi E_P \delta} \int_0^{\delta} \sqrt{\frac{\delta - r}{r}} \, dr \, dz \\ &= \frac{1}{E_P} \int_0^{t_P} K^2(z) \, dz. \end{aligned} \tag{9}$$

Therefore, the total strain energy release rate can be expressed in terms of the root-mean-square value of K as follows:

$$G = \frac{K_{\text{rms}}^2}{E_P}, \tag{10}$$

where K_{rms} is given by

$$K_{\text{rms}} = \left(\frac{1}{t_P} \int_0^{t_P} K^2(z) \, dz \right)^{1/2}, \tag{11}$$

where subscript rms refers to root-mean-square of the stress intensity factor across the crack front. It is noted that K_{rms} is not equal to the thickness average of the stress intensity factor K_{mean}. Instead, for a linear distribution as in eqn (8), it follows from eqn (11) that

$$K_{\text{rms}}^2 = K_{\text{mean}}^2 + \tfrac{1}{3} K_b^2 \equiv \tfrac{1}{3}(K_{\min}^2 + K_{\min} K_{\max} + K_{\max}^2). \tag{12}$$

It is seen that the root-mean-square value is greater than the arithmetic mean. As will be shown later, eqn (12) furnishes an important relationship for calculating the maximum stress intensity factor, as K_{rms} can be determined from energy considerations.

4. FINITE ELEMENT ANALYSIS

Because a one-sided bonded repair represents a complex three-dimensional, layered system, especially with the presence of a finite size crack in one layer only, a rigorous analytical solution would be intractable. Therefore, a finite element analysis is conducted first. This will at least serve to clarify the question of whether the stress intensity factor for a one-sided repaired crack remains bounded. To this end, a three-dimensional finite element model has been developed for an isotropic, centre-cracked panel repaired with an isotropic reinforcement using the commercial software package PAFEC (1995). To facilitate comparison with the earlier work of Arendt and Sun (1994), the reinforcement is assumed to be isotropic (rather than orthotropic, as would be more appropriate for the uni-directional fibre composite patches used in practice), and the same values that were used by Arendt and Sun for the elastic constants and the thicknesses will be used here, as summarized in Table 1. These are representative of values for an aluminium plate repaired by a boron/epoxy patch, using an epoxy-based structural adhesive.

The finite element mesh is shown in Fig. 2(a). In all cases to be discussed in the following, only a quadrant of the plate was modelled. No debond between the plate and the reinforcement is considered.

The three constituents in Fig. 1, the plate, the adhesive layer and the reinforcing patch, are assumed to deform elastically only, and are each modelled by 20-noded isoparametric brick elements. One important issue that needs to be addressed is how to deal with a relatively thin adhesive layer, which is typically an order of magnitude thinner than the plate or the patch (see Table 1). To this end, the technique of reduced integration is now well established for dealing with the problem of large aspect ratios for elements in modelling thin layers. To determine K, isoparametric wedge-shaped elements have been employed around the crack tip node, as indicated in Fig. 2(b), with the mid-point nodes shifted to quarter-point locations to capture the characteristic crack-tip singularity. To validate the adequacy of the FE mesh, calculations were first carried out for an unpatched plate. The results, as depicted in Fig. 3, were found to agree within 2% with the handbook values for this case (Murakami, 1987), for half-crack lengths ranging from 10 to 170 mm.

For the repaired plate, the results for a two-sided repair were obtained by using a symmetry restraint on the plane $z = 0$, as indicated in Fig. 1(b). The stress intensity factor was determined for a large number of half-crack lengths ranging from 2 to 170 mm. These calculations were then repeated for the case of a one-sided repair by removing the symmetry restraint on $z = 0$. The results are shown in Fig. 4, where the stress intensity factor for one-sided repair was determined from the finite element results using eqn (7b). It is apparent from Fig. 4 that the stress intensity factor for a one-sided repair significantly exceeds the value for the corresponding two-sided repair, indicating that the secondary bending induced by the load–path eccentricity has a significant detrimental effect on the efficiency of bonded reinforcement. It is noted that K_{rms} obtained from the present three-dimensional finite element analysis is in good agreement with those obtained by Arendt and Sun (1994), who modelled the deformation of the cracked plate and the reinforcement using Mindlin plate theory, with the two plates being coupled by distributed shear and tension springs representing the adhesive layer. One important feature of the numerical results is that the stress intensity factor in the one-sided repair case does not increase beyond a limiting value, but increases monotonically towards an asymptotic value. The solid line shown in the figure represents the analytical prediction of the upper bound, which will be derived in the next section.

Table 1. Dimensions and material properties of a typical repair

Layer	Young's modulus (GPa)	Poisson's ratio	Thickness (mm)	Height (mm)	Width (mm)
Plate	71	0.3	3.0	500	500
Reinforcement	207	0.3	1.02	100	500
Adhesive	1.89	0.33	0.203	100	500

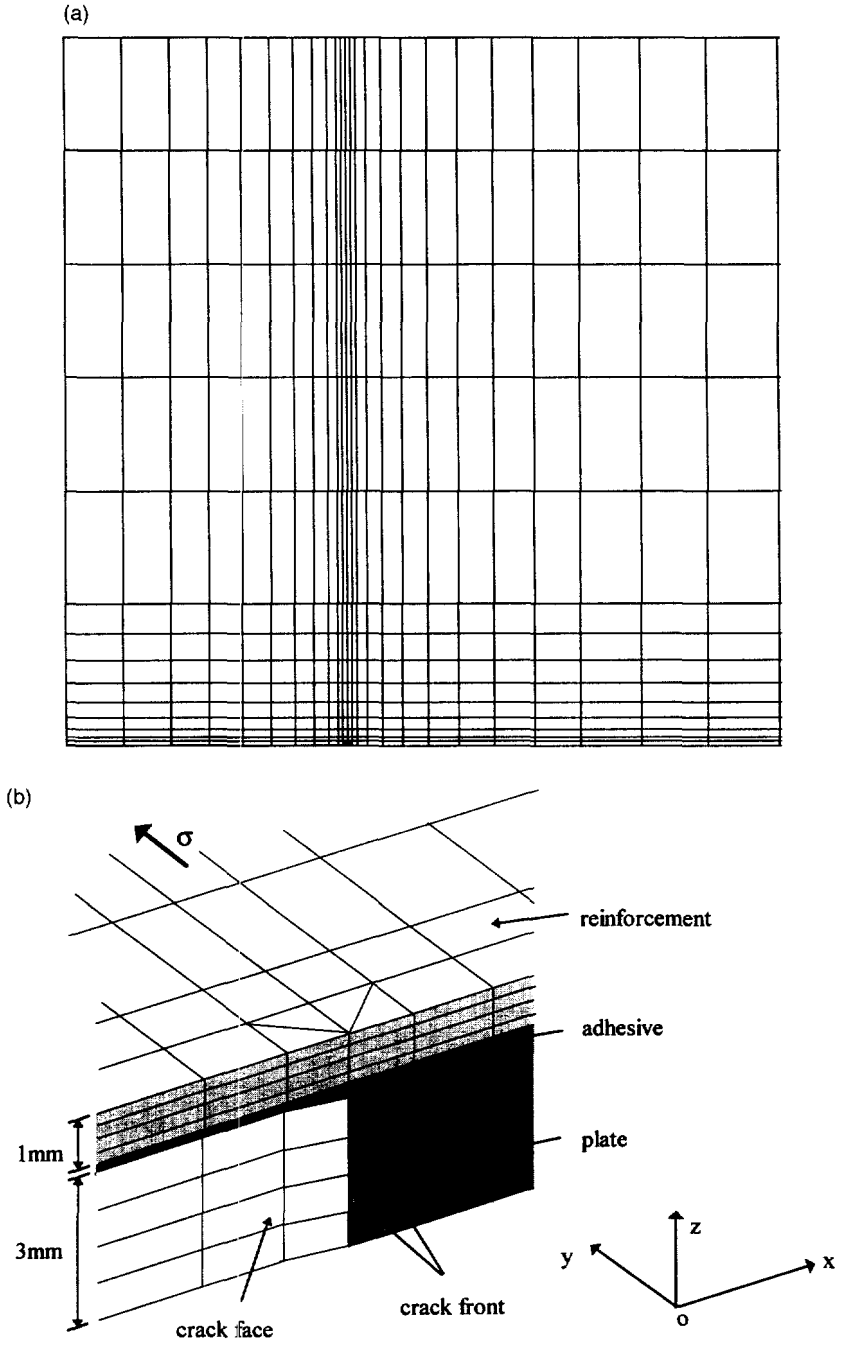

Fig. 2. Finite element mesh for a cracked plate repaired with reinforcement: (a) plan view; and (b) near crack tip.

The through-thickness variation of the stress intensity factor $K(z)$ for a relatively long crack length (100 mm) is shown in Fig. 5, compared with the analytical prediction to be presented later. It is seen that the stress intensity factor clearly follows a linear variation across plate thickness, consistent with the expectation from a shear-deformation plate theory. The solid line shown in the figure is again the theoretical prediction to be discussed in Section 5. It is known that the stress singularity at the intersection of a crack front with a free surface differs from the standard inverse-square-root singularity (except for zero Poisson's ratio) and, therefore, cannot be characterized by K (Benthem, 1977). Nevertheless, the prediction of a linear variation of K across the crack front as in eqn (8) by shear-deformation plate theories appears to be quite accurate for all practical purposes (Hui and

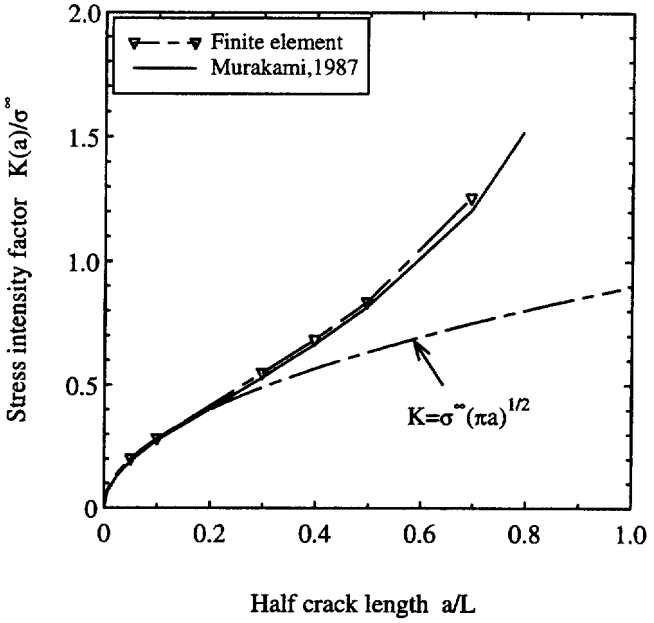

Fig. 3. Comparison between finite element solution and analytical solution for a centre-cracked plate under tension.

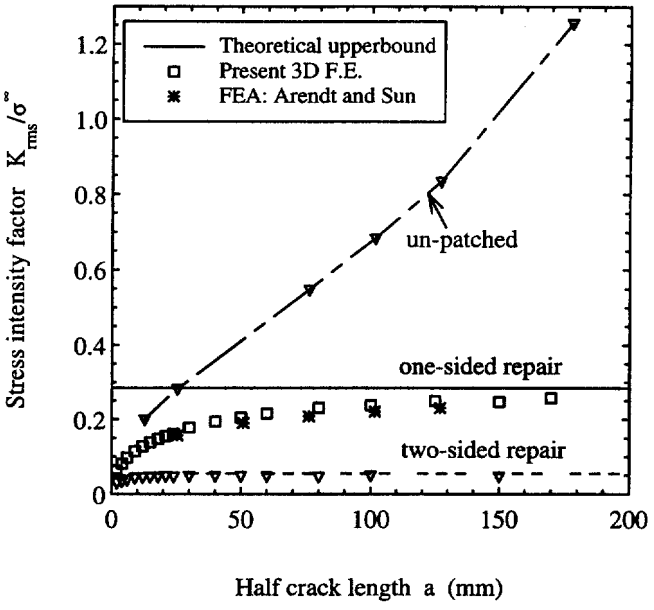

Fig. 4. Stress intensity factors vs crack length for two- and one-sided repairs. Symbols—three-dimensional finite element results; dashed line—eqn (1); solid line—eqn (45).

Zehnder, 1993). It is also noted that from Fig. 5 there is a significant variation of K across the thickness, contrary to a claim by Arendt and Sun (1994) that it is negligible.

5. ANALYTICAL APPROACH

In the following we will focus on the derivation of the upper bound for the stress intensity factor, which corresponds to the limiting value for semi-infinite crack length. For the sake of simplicity, we assume the structure is stress-free before an external load is applied, although the analysis can be readily extended to include the effect of thermal residual stress. By definition, the strain energy release rate, $G = -\delta\Pi/\delta a$, where Π represents the potential energy of a cracked system. For a *linear elastic* structure, the strain

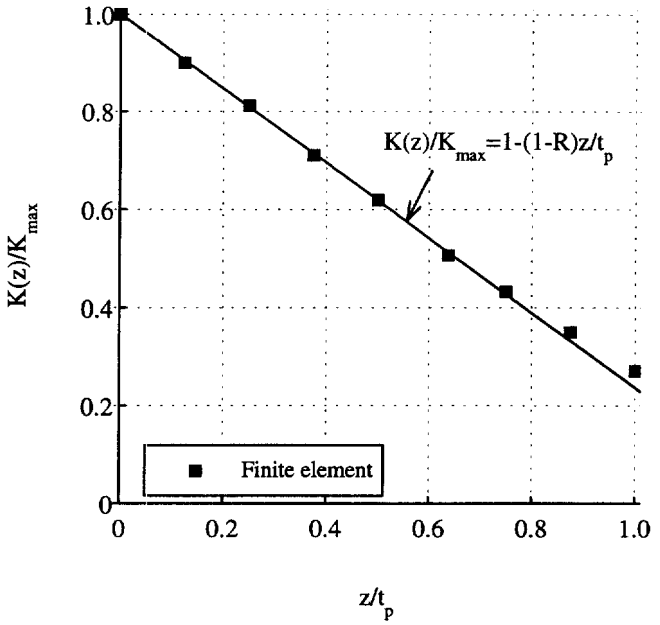

Fig. 5. Distribution of stress intensity factor along crack front ($R = 0.236$).

energy release rate is equal to the change in total strain energy during a virtual crack extension of unit length. Following the reasoning in Rose (1981), for a semi-infinite crack the stress and displacement fields after a virtual crack extension of unit length are unchanged, but shifted to the right by a unit distance, which in essence amounts to a vertical strip of unit width with the cross-section depicted in Fig. 1(d) being converted into one of the same width, but with the cross-section shown in Fig. 1(c). The energy gained by the system during this virtual crack extension is denoted by δU_E. From the theory of elasticity, δU_E is also equal to the work extracted by relaxing to zero the tractions, $\sigma_{yy}(x \to \infty, y = 0, z)$, through the displacement, $u_y(x = 0, y = 0^+, z)$ on the plate depicted in Fig. 1(a). Provided the strip shown in Fig. 1(c) can support the applied stress, the displacement $u_y(x = 0, y = 0^+, z)$ in Fig. 1(a) or (b) will be finite, so that δU_E and G_∞, will also be finite.

Within the framework of a geometrically linear analysis, the strain energy release rate, G_∞ can be determined by a two-stage approach as advocated by Rose (1981, 1982, 1988) for two-sided repairs. First of all, the stress distribution in the un-cracked plate, $\sigma_{yy}(y = 0, z)$ depicted in Fig. 1(d), is determined, and secondly, the displacement $u_y(y = 0^+, z)$ is obtained for the representative bonded joint shown in Fig. 1(c). In particular, the upper bound of stress intensity factor can be determined as follows. A cut is introduced in the plate along the line segment ($y = 0, 0 \leqslant z \leqslant t_p$) and the stress σ_{yy} relaxed to zero, giving rise to a crack-face displacement $u_y(y = 0, z)$. The work extracted during this process is the energy change δU_E required to calculate the strain energy release rate:

$$G_\infty = -\frac{\partial \Pi}{2t_p\,\partial a} = \frac{1}{2t_p\,\delta a} 2\int_0^{\delta a}\int_0^{t_p} \frac{1}{2}\sigma_{yy}(y = 0, z)\cdot 2u_y(y = 0^+, z)\,\mathrm{d}z$$

$$= \frac{1}{t_p}\int_0^{t_p} \sigma_{yy}(y = 0, z)u_y(y = 0^+, z)\,\mathrm{d}z. \tag{13}$$

5.1. *Stage one: reinforcement of uncracked plate*

In the following analysis the height of the reinforcement is assumed to be far greater than the shear stress transfer length, β^{-1}, so that the influence of the outer edge of the reinforcement can be neglected, and the overlap region can be treated as a composite plate with a rigid bondline as in Goland and Reissner (1944). The equivalent membrane force,

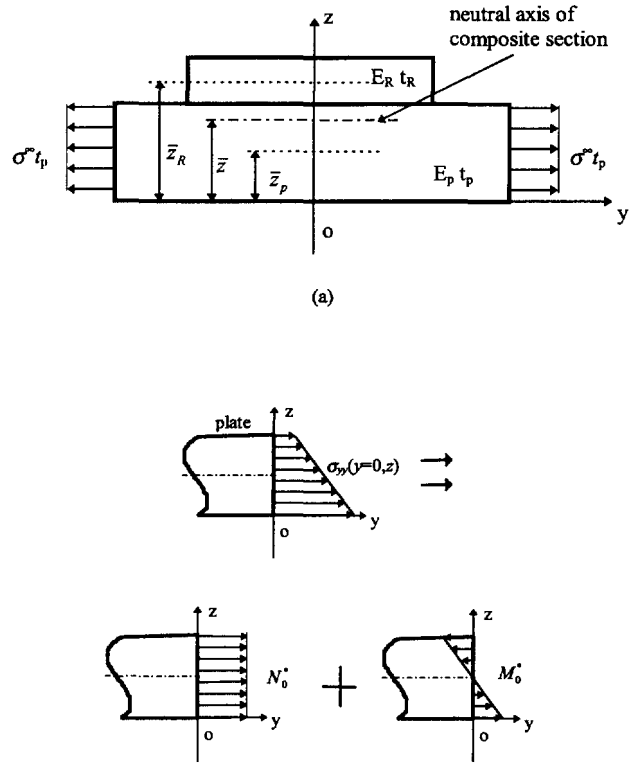

Fig. 6. Stress distributions in an uncracked bonded reinforcement: (a) composite beam subjected to asymmetric loading; (b) stress distribution in the plate.

N, and bending moment, M, acting on the composite plate (or beam) are, adopting usual sign conventions:

$$N = \sigma^\infty t_p \tag{14}$$

$$M = \sigma^\infty t_p(\Delta t), \tag{15}$$

where

$$\Delta t = \bar{z} - \bar{z}_p, \tag{16}$$

where $\bar{z}$ and $\bar{z}_P$ denote, respectively, the distance between the unbonded surface to the neutral axes of the composite plate and the plate; see Fig. 6(a). The term Δt signifies the shift of the neutral axis. From the composite beam theory [e.g. see Gere and Timoshenko (1987)], the distance between neutral axis of the section and the lower surface plate is:

$$\bar{z} = \frac{E'_p t_p \bar{z}_p + E'_R t_R \bar{z}_R}{E'_p t_p + E'_R t_R} = \frac{\bar{z}_p + S\bar{z}_R}{1+S}, \tag{17}$$

where $\bar{z}_P(=t_P/2)$ and $\bar{z}_R(=t_P+t_A+t_R/2 \cong t_P+t_R/2)$ denote, respectively, the distance between the lower surface to the neutral axes of the plate and the reinforcement, as indicated in Fig. 6(a). The total moment of inertial for the composite section under plane strain conditions is:

$$I_t = I_p + nI_R, \tag{18}$$

where $n = E'_R/E'_P$, and

$$I_p = \frac{1}{12}t_p^3 + t_p(\bar{z}_p - \bar{z})^2, \tag{19}$$

$$I_R = \frac{1}{12}t_R^3 + t_R(\bar{z}_R - \bar{z})^2. \tag{20}$$

With the conventional assumption of plane section remaining plane and normal to the neutral axis (classical plate theory), the normal strain distribution in the plate is given by:

$$\varepsilon_{yy}(y = 0, z) = \frac{N}{E'_P t_P + E'_R t_R} + \frac{M}{E'_P I_t}(\bar{z} - z). \tag{21}$$

According to Hooke's law the normal stress in the plate $\sigma_{yy}(y = 0, z)$ is thereby

$$\sigma_{yy}(y = 0, z) = \frac{\sigma^\infty}{1+S} + \frac{\sigma^\infty t_p(\Delta t)(\bar{z} - z)}{I_t} \quad (0 < z < t_P). \tag{22}$$

To facilitate the following analysis, it is convenient to express this stress distribution in terms of a membrane force N_0^*, and a bending moment, M_0^*, as illustrated in Fig. 6(b),

$$N_0^* \equiv t_P\sigma_0^* = -\int_0^{t_P} \sigma_{yy}(y = 0, z)\,dz = \frac{\sigma^\infty t_P}{1+S} + \frac{\sigma^\infty t_P^2(\Delta t)^2}{I_t} \tag{23}$$

and

$$M_0^* \equiv \frac{\sigma_b t_P^2}{6} = -\int_0^{t_P} \sigma_{yy}(y = 0, z)(z - \bar{z}_p)\,dz = \frac{\sigma^\infty t_p^4(\Delta t)}{12I_t}. \tag{24}$$

Comparison between eqns (23) and (2) clearly shows that the plate in a one-sided repair is transferring more stress than in an equivalent two-sided repair (or fully supported one-sided repair). Therefore, due to the out-of-plane bending induced by load eccentricity, the stress distribution along the prospective crack path before the crack appears is higher than for a corresponding two-sided reinforcement. In addition, there is a bending moment acting on the prospective crack faces. Consequently, due to the shift of neutral plane, one-sided repairs would experience not only an increase in the net force that the plate is transmitting, but also a secondary bending moment. It can, therefore, be expected that both the higher membrane force and the additional bending moment will contribute to a higher energy being released than in two-sided repairs, giving rise to a higher strain energy release rate.

5.2. *Stage two: deformation of the representative bonded joint*

Now that the stress distribution at the prospective crack location has been determined, the crack face opening displacement is the only remaining unknown. The representative

bonded joint to be considered is depicted in Fig. 7(a, b), with coordinates and notations. A schematic drawing of the one-sided reinforcement after the introduction of a crack is shown in Fig. 7(c), where the deflection of the plate and reinforcement are somewhat exaggerated for greater clarity. The deformed mesh from a geometrically linear finite element analysis is shown in Fig. 7(d). For symmetry, only half of the joint is shown. The bending moment acting on the reinforcement at the centre is

$$M_m = \sigma^\infty t_p \frac{t_p + t_R}{2}. \tag{25}$$

The governing equation for the shear stress τ_A in the adhesive layer is, similar to single lap joints (Goland and Reissner, 1944), with the relevant sign conventions being indicated in Fig. 7(b),

$$\frac{d^3\tau_A}{dy^3} - \beta_s^2 \frac{d\tau_A}{dy} = 0 \tag{26}$$

where $\beta_s = 2\beta$ for single strap joints. Here β^{-1} is the shear stress transfer length for two-sided reinforcement as given by eqn (4). For a semi-infinite overlap joint in the domain $(0 \leqslant y < \infty)$, the relevant solution for the shear stress is

$$\tau_A(y) = \tau_{A,max}\, e^{-\beta_s y} \tag{27}$$

where $\tau_{A,max}$ represents the maximum shear stress at $y = 0$. The boundary condition for the shear stress is:

$$t_A \frac{d\gamma_A}{dy}\bigg|_{y=0} = \frac{N}{E'_R t_R} + \frac{6M_m}{E'_R t_R^2}, \tag{28}$$

therefore, the maximum adhesive shear strain is, noting eqn (25) and $\beta_s = 2\beta$

$$\gamma_{A,max} = -\left[\frac{N}{E'_R t_R} + \frac{6M_m}{E'_R t_R^2}\right]\frac{1}{t_A \beta_s} = -\frac{\sigma^\infty}{SE'_P \beta t_A}\left(2 + \frac{3}{2}\frac{t_P}{t_R}\right). \tag{29}$$

It is noted that the term $\sigma^\infty / SE'_P \beta t_A$ represents the maximum adhesive shear strain in two-sided repair (Rose, 1988). Thus it is clear that one-sided repairs experience a much higher adhesive shear strain, when compared with an equivalent two-sided repair (or a fully supported one-sided repair). This increase in adhesive shear strain would result in larger crack opening, hence higher stress intensity factors. The main factor leading to the higher shear strain is the localised bending of the reinforcement resulting from load-path eccentricity; this is represented by the second term in the bracket of the above equation.

Similarly the governing equation for the peel stress σ_A in the adhesive layer is (Hart-Smith, 1982):

$$\frac{d^4\sigma_A}{dy^4} + 4\kappa^4 \sigma_A = 0, \tag{30}$$

where κ is given by

$$\kappa^4 = \frac{E'_A}{4t_A}\left(\frac{1}{D_P} + \frac{1}{D_R}\right), \tag{31}$$

where D_P and D_R refer to the bending stiffness of the plate and reinforcement,

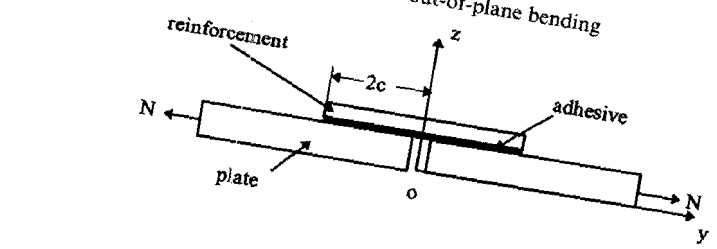

(a)

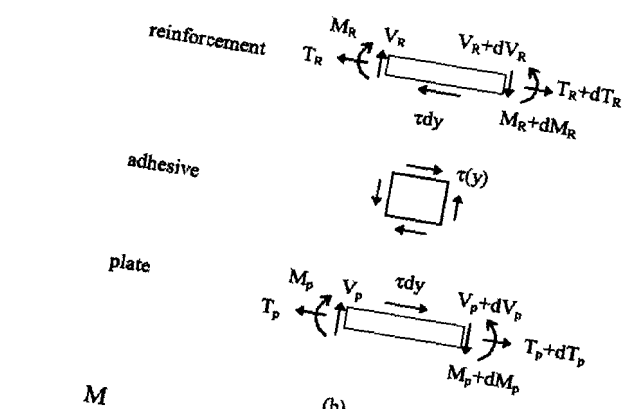

(b)

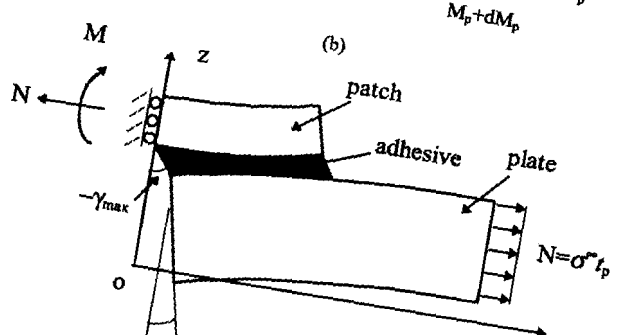

(c)

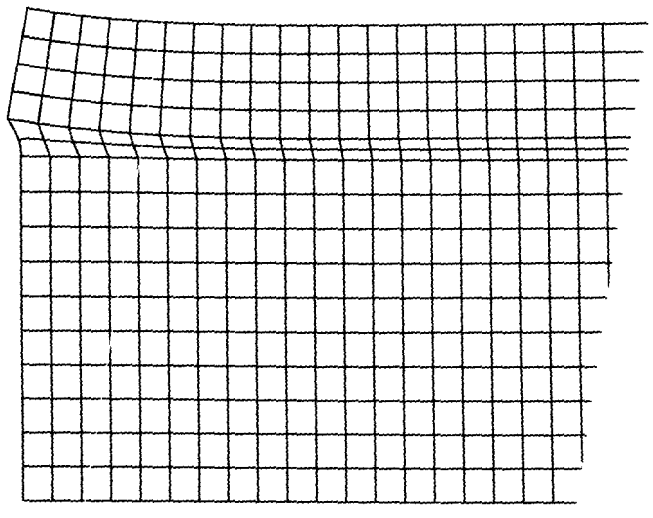

(d)

Fig. 7. A single strap joint representing one-sided repair: (a) geometry and coordinates for undeformed shape; (b) sign conventions; (c) opening of crack due to adhesive and plate deformation; and (d) a deformed finite element mesh of representative single strap joint.

$D_{P,R} = E'_{P,R} t^3_{P,R}/12$. The relevant solution for the peel stress in the case of a semi-infinite overlap in the domain $(0 \leqslant y < \infty)$ is:

$$\sigma_A(y) = (A \cos \kappa y + B \sin \kappa y)\, e^{-\kappa y}, \tag{32}$$

where A and B are two unknown constants yet to be determined from boundary conditions at $y = 0$, which are,

$$\left.\frac{d^2\sigma_A}{dy^2}\right|_{y=0} = \frac{E'_A}{t_A}\frac{d^2(w_R - w_P)}{dy^2} = \frac{E'_A}{t_A}\left(\frac{M_R(y=0)}{D_R} - \frac{M_P(y=0)}{D_P}\right)$$

$$= \frac{E'_A M_m}{t_A D_R} \tag{33a}$$

and

$$\left.\frac{d^3\sigma_A}{dy^3}\right|_{y=0} = \frac{E'_A}{t_A}\frac{d^3(w_R - w_P)}{dy^3} = \frac{E'_A}{t_A}\left(\frac{V_R + \tau_{A,max} t_R/2}{D_R} - \frac{V_P + \tau_{A,max} t_P/2}{D_P}\right)$$

$$= \frac{E'_A}{t_A}\left(\frac{6}{E'_R t_R^2} - \frac{6}{E'_P t_P^2}\right)\tau_{A,max} \tag{33b}$$

where use has been made of the following boundary conditions: (i) V_R at $y = 0$ is equal to zero because of symmetry; (ii) at the free surface ($y = 0$) V_P and M_P are both zero.

It is also easy to show the following relationships:

$$\frac{d\sigma_A}{dy} = -\kappa[(A+B)\sin \kappa y + (A-B)\cos \kappa y]\, e^{-\kappa y} \tag{34a}$$

$$\frac{d^3\sigma_A}{dy} = 2\kappa^2[A \sin \kappa y - B \cos \kappa y]\, e^{-\kappa y} \tag{34b}$$

$$\frac{d^3\sigma_A}{dy^3} = -2\kappa^3[(A-B)\sin \kappa y - (A+B)\cos \kappa y]\, e^{-\kappa y}. \tag{34c}$$

Combining eqns (33a) an (34b), we have

$$-2\kappa^2 B = \frac{E'_A M_m}{t_A D_R},$$

similarly after combining eqns (33b) and (34c),

$$2\kappa^3(A+B) = \frac{E'_A}{t_A}\left(\frac{6}{E'_R t_R^2} - \frac{6}{E'_P t_P^2}\right)\tau_{A,max}, \tag{35}$$

thus one finds that

$$\kappa(A-B) = \frac{E'_A M_m}{t_A \kappa D_R} + \frac{E'_A}{\kappa^2 t_A}\left(\frac{3}{E'_R t_R^2} - \frac{3}{E'_P t_P^2}\right)\tau_{A,max}, \tag{36}$$

so that, noting eqn (34a)

$$\left.\frac{d\varepsilon_A}{dy}\right|_{y=0} = -\frac{\kappa(A-B)}{E'_A} = -\frac{M_m}{t_A\kappa D_R} - \frac{1}{2\kappa^2 t_A}\left(\frac{6}{E'_R t_R^2} - \frac{6}{E'_P t_P^2}\right)\tau_{A,max}, \tag{37}$$

Let us denote the rotation of the plate at $y = 0$ as θ_0. Since $\varepsilon_A = (w_R - w_P)/t_A$, we have

$$\begin{aligned}\theta_0 &= \left.\frac{\partial w_P}{\partial y}\right|_{y=0} = -\left.\frac{\partial(w_R - w_P)}{\partial y}\right|_{y=0} = -t_A\left.\frac{\partial \varepsilon_A}{\partial y}\right|_{y=0} \\ &= \frac{M_m}{\kappa D_R} + \left(\frac{3}{E'_R t_R^2} - \frac{3}{E'_P t_P^2}\right)\frac{\gamma_{A,max}\mu_A}{\kappa^2} \\ &= \frac{6\sigma^\infty t_P(t_P + t_R)}{\kappa E'_R t_R^3}[1 - Q],\end{aligned} \tag{38}$$

where the symmetry condition $\partial w_R/\partial y|_{y=0} = 0$ has been used, and

$$Q = \frac{\beta}{\kappa(1+S)}\frac{(t_R/t_P + 3/4)(1 - St_R/t_P)}{1 + t_R/t_P}. \tag{39}$$

In the case of identical reinforcement, i.e. the patch and the cracked plate have the same moduli and thicknesses ($S = 1$ and $t_R = t_P$), we have $Q = 0$. In general, Q is far less than unity for typical repairs. For instance, $Q = 0.08054$ for the repair configuration discussed in Section 3.

The plate displacement in the y direction at coordinate z can be expressed as, referring to Fig. 7(c):

$$u_y(y = 0^+, z) = -\gamma_{A,max}t_A + \theta_0(t_P - z). \tag{40}$$

Thus, the displacement along the mid-plane of the cracked plate is:

$$u_0 = -\gamma_{A,max}t_A + \theta_0 t_P/2, \tag{41}$$

which also represents the average displacement through the plate thickness. A comparison between the theoretical prediction and the finite element results of a representative single strap joint is shown in Fig. 8, demonstrating a reasonable agreement.

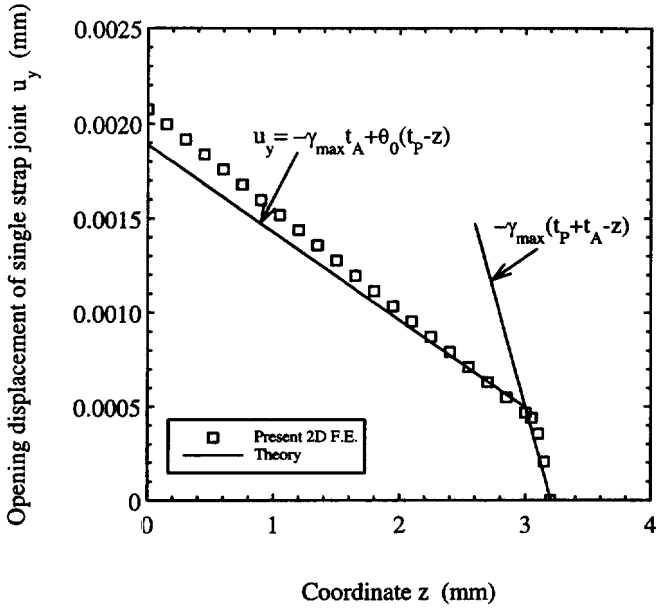

Fig. 8. Comparison between theory and finite element results for the representative single strap joint.

5.3. *Strain energy release rate and stress intensity factors*

As indicated earlier, see eqn (13), the strain energy release rate G^*_∞ can be evaluated as the work extracted (per unit thickness, per unit crack advance) on allowing the stage one stress $\sigma_{yy}(y=0,z)$ given by eqn (22) to relax to zero through the displacement $u_y(y=0^+,z)$ in eqn (40). It can be easily shown that the strain energy release rate can be written alternatively in terms of the membrane force and the bending moment:

$$t_P G^*_\infty = N^*_0 u_0 + M^*_0 \theta_0. \tag{42}$$

Here the superscript "*" refers to one-sided repair. Therefore,

$$G^*_\infty = \frac{(\sigma^\infty)^2}{(1+S)S\beta E'_P}\omega^2, \tag{43}$$

where ω signifies a bending correction factor and is given by

$$\omega^2 = 2+\frac{3t_P}{2t_R}+\frac{3\beta t_P}{\kappa t_R}\left(1+\frac{t_P}{t_R}\right)(1-Q)+(1+S)\left(2+\frac{3t_P}{2t_R}\right)\left(\frac{\Delta t}{t_P}\right)^2\frac{t_P^3}{I_t}$$
$$+(1-Q)(1+S)\frac{\beta}{\kappa}\left(1+\frac{t_P}{t_R}\right)\frac{t_P}{t_R}\frac{\Delta t}{t_P}\frac{t_P^3}{I_t}\left(\frac{3\bar{z}}{t_P}-1\right). \tag{44}$$

Here the bending correction factor ω represents the bending effect due to the shift of neutral axis in the case of one-sided repair. Referring to eqn (10), the root-mean-square stress intensity factor for one-sided reinforcement can be expressed as:

$$K^*_{\infty,\mathrm{rms}} = \sqrt{E_P G^*_\infty} = k_\infty \omega, \tag{45}$$

where K_∞ denotes the asymptotic stress intensity factor for two-sided repair. The calculated asymptotic values for $K^*_{\infty,\mathrm{rms}}$ are shown in Fig. 9, together with the finite element results,

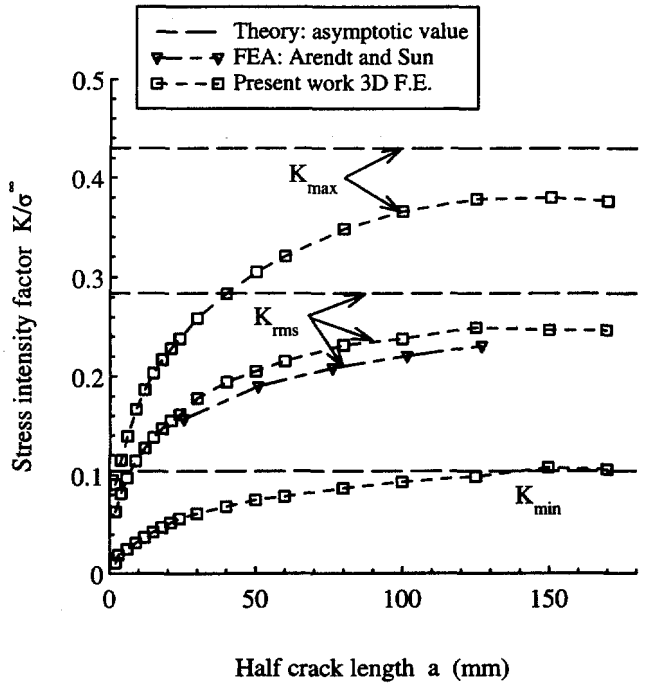

Fig. 9. Comparison between analytical solution and finite element results for one-sided reinforcement. Symbols—three-dimensional finite element results; dashed lines—theoretical predictions of upper bound.

confirming that the analytical solution is truly an upper bound and, therefore, provides a *conservative* estimate of for design purposes.

Although the root-mean-square of the stress intensity factor has been derived, the maximum and minimum stress intensity factors, which are related through eqn (12), still remain unresolved. An additional equation is required to partition the total strain energy release rate into membrane and bending components. A related study (Wang and Rose, 1997b) has shown that the energy method alone is insufficient to determine the membrane and bending stress intensity factors. However, it is not unreasonable to assume that the ratio between the minimum and maximum stress intensity factor is independent of crack length, which can, therefore, be readily evaluated in the short crack limit, $a \to 0$. In this case, the membrane and bending stress intensity factors are linearly related to the membrane and bending stresses which would prevail in a patched, but uncracked, plate. It is interesting to note that, for a cracked plate subjected to bending and in-plane extension, both the Kirchhoff plate theory and Reissner's shear deformation theory would yield the same solution in the short crack limit (Sih, 1971), i.e. $K_m = \sigma_m\sqrt{\pi a}$ and $K_b = \sigma_b\sqrt{\pi a}$. Here K_m and K_b represent, respectively, the membrane and bending stress intensity factors, and σ_m and σ_b are the membrane and maximum bending stresses. Based on the afore-mentioned hypothesis, the ratio between the minimum and the maximum stress intensity factors can be expressed as, noting equation (22)

$$R = \frac{K_{min}}{K_{max}} \equiv \frac{\sigma_m - \sigma_b}{\sigma_m + \sigma_b} = \frac{I_t + (1+S)t_p(\Delta t)(\bar{z} - t_P)}{I_t + (1+S)t_P(\Delta t)\bar{z}}. \tag{46}$$

Together with eqn (12), the maximum and minimum stress intensity factors can now be determined, where $K^*_{\infty,rms}$ is given by eqn (45). The respective formulae for the minimum and maximum stress intensity factors are given below for completeness,

$$K^*_{\infty,max} = \left(\frac{3}{1+R+R^2}\right)^{1/2} K^*_{\infty,rms} \tag{47}$$

and

$$K^*_{\infty,min} = \left(\frac{3}{1+R+R^2}\right)^{1/2} RK^*_{\infty,rms}. \tag{48}$$

The calculated asymptotic values for $K^*_{\infty,max}$ and $K^*_{\infty,min}$ are also depicted in Fig. 9, together with the finite element results. To demonstrate the validity of the hypothesis, the finite element results for $K^*_{\infty,rms}$ and $K^*_{\infty,max}$ are plotted in Fig. 10(a). Also plotted in the figure are the results reported by Jones (1983). The stress ratios R determined from eqn (46) is equal to 0.236 for the repair configuration considered in Section 4. As shown in Fig. 10(a), there is a good correlation between the finite element results and eqn (47), represented by the solid line. Furthermore, the ratios between $K^*_{\infty,rms}$ and $K^*_{\infty,max}$ for various crack lengths are presented in Fig. 10(b), confirming the above hypothesis that the membrane to bending stress intensity factor ratio is independent of crack length. It should be noted that the problem can be analysed more rigorously using a line spring method (Wang and Rose, 1997c).

It is now possible to define a spring constant for one-sided repairs so that the stress intensity factors can be expressed in a similar form as in two-sided repairs,

$$k^* = \left(\frac{\sigma^*_{rms}}{K^*_{\infty,rms}}\right)^2 \tag{49}$$

where $\sigma^*_{rms} = [(\sigma^*_0)^2 + \sigma_b^2/3]^{1/2}$, representing the root-mean-square of the prospective stress

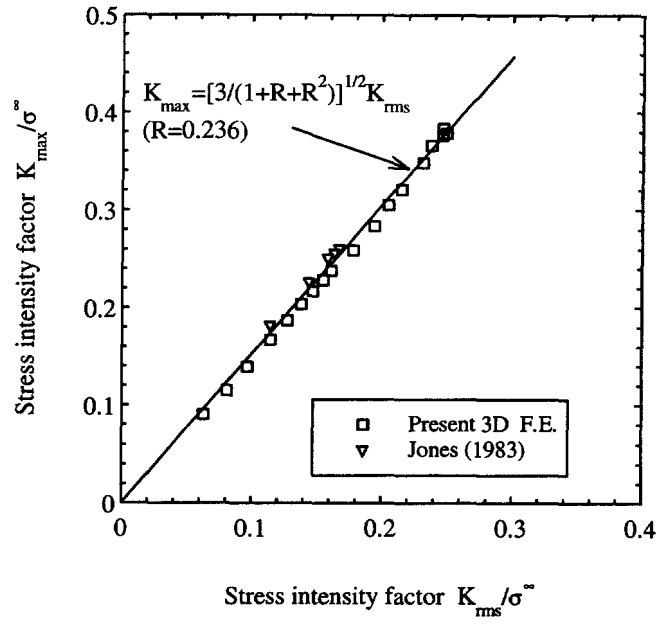

(a)

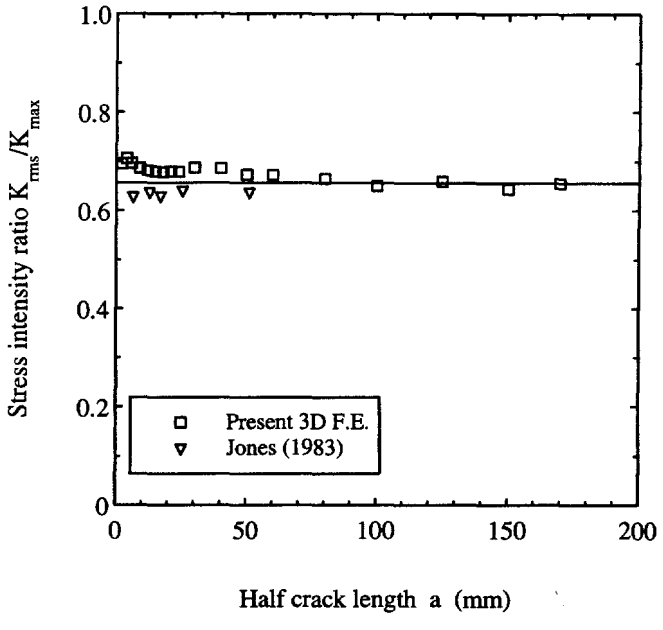

(b)

Fig. 10(a) Correlation between the maximum stress intensity factor $K^*_{\infty,max}$ and the root-mean-square stress intensity factor $K^*_{\infty,rms}$; (b) ratio of $K^*_{\infty,rms}/K^*_{\infty,max}$ vs crack length.

distribution across the crack front. Here σ_0^* and σ_b are, respectively, given by eqns (23) and (24).

5.4. *Interpolation between short and long crack limits*

Having obtained the asymptotic behaviour of the stress intensity factors in the long crack ($a \to \infty$) limit, it would be useful for engineering application to construct an interpolation formula for intermediate crack lengths. Here, let us adopt the interpolating formula for two-sided repairs (Rose, 1982; Wang and Rose, 1997a), which has been shown to agree well with exact, numerical solutions of integral equations. The mean stress intensity factor can be expressed as:

$$K_{\text{rms}}(a) = \sigma^*_{\text{rms}}\sqrt{\pi a}F(k^*a) \tag{50}$$

where

$$F(x) = \left(\frac{\tanh(\pi x/(1+A\pi x))}{\pi x}\right)^{1/2}, \tag{51}$$

where constant A (equal to 0.3 for $S = 1$ and equal to 0.1 for $S \to \infty$) was determined by fitting the exact solutions of the integral equation representing two-sided repairs (Wang and Rose, 1997a). Using eqns (47) and (48), the maximum and minimum stress intensity factors can be readily evaluated.

6. PARAMETRIC STUDIES

For both the symmetric and asymmetric bonded reinforcements, the asymptotic stress intensity factors are dependent on a large number of parameters pertaining to the three constituents. For a given cracked plate, there are at least four main variables affecting the limiting stress intensity factor: the Young's moduli and thickness of the patch and the adhesive layer. However, the stress intensity factor for symmetric reinforcement can be rewritten as:

$$K_\infty = \sigma^\infty\sqrt{t_{\text{P}}}\left(\frac{F}{S(1+S)^3}\right)^{1/4}\sqrt{1-\nu_{\text{P}}^2}, \tag{52}$$

where $F = E'_{\text{P}}t_{\text{A}}/\mu_{\text{A}}t_{\text{P}}$. This formula shows clearly two important non-dimensional parameters, which are: (i) the stiffness ratio, S; (ii) the flexibility ratio, F. For most practical repairs, the flexibility ratio F is typically of the order of unity, e.g. $F = 6.7$ for the repair geometry shown in Table 1, while S is designed to be close to unity.

In the case of one-sided reinforcement, a similar parametric analysis is much more complicated. Nevertheless, after normalization (see Appendix A), the bending correction factor ω can be shown to depend on three non-dimensional parameters plus the Poisson's ratio of the adhesive layer, i.e.

$$\omega = \omega(F, S, T, \nu_{\text{A}}) \tag{53}$$

where $T = t_{\text{P}}/t_{\text{R}}$.

A non-dimensional plot of the bending correction factor for the balance repair configuration, i.e. $S = 1.0$, is shown in Fig. 11(a), demonstrating a monotonic decline as the thickness of the reinforcement increases, irrespective of the flexibility ratio F. Therefore, thicker reinforcements are beneficial in reducing the effect of out-of-plane bending. Up until now, bonded patches have been designed to balance the stiffness (Baker and Jones, 1988), i.e. the extensional stiffness of the reinforcement is the same as that of the plate ($S = 1.0$). Such designs, however, appear to be chosen for convenience rather than based on any theoretical considerations. From the present analysis, it is clear that by selecting patches having the same thickness or even greater thickness than the cracked plate, significant reduction in the bending effect can be achieved.

From Fig. 11(a), it is clear that in the case of unidirectional boron composite patches, a reduction of more than 50% in the bending effect can be obtained by employing a reinforcement with a thickness ratio greater unity. This, in practice, can be easily achieved by adopting crossply laminates to increase the thickness while maintaining the overall extensional stiffness. Naturally, there are other considerations concerning the design of a reinforcement patch, not least of which is the ultimate strength of a patch. In this regard, since there is a localized stress concentration in the reinforcement over the crack region due

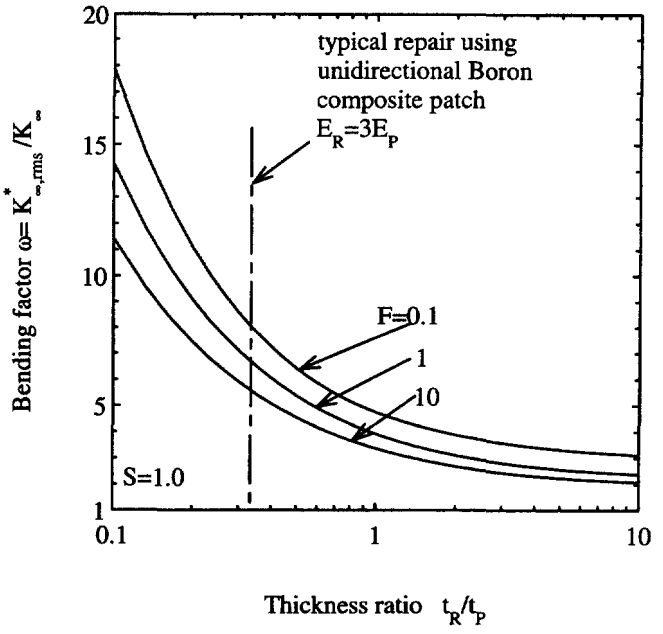

(a)

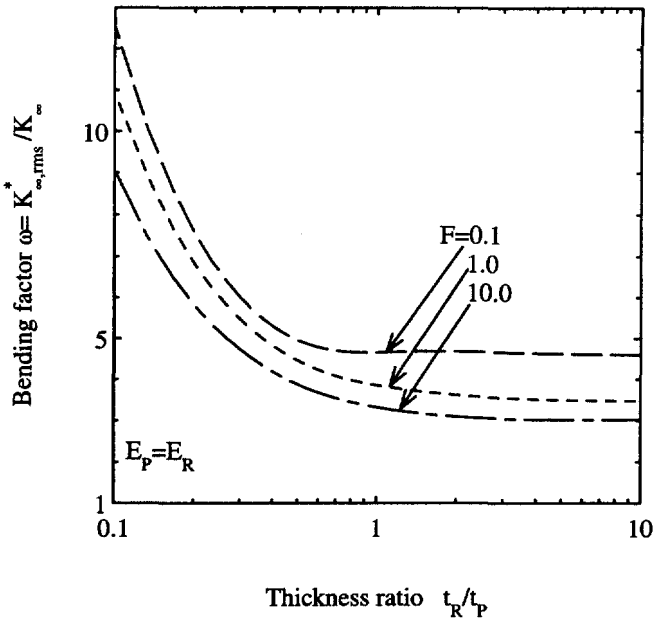

(b)

Fig. 11. Influence of reinforcement thickness on bending correction factor for: (a) balanced reinforcement ($S = 1.0$); (b) fixed modulus ratio $E_P = E_R$; (c) fixed modulus ratio $E_R = 3E_P$.

to localized bending, a thicker reinforcement would have an additional benefit of reducing the stress concentration, thus enhancing the patch strength.

The thickness influences for other modulus ratios are presented in Fig. 11(b, c) for E_R/E_P equal to 1 and 3, respectively. It is clear that for identical modulus, any further increase in the thickness ratio beyond unity does not seem to reduce out-of-plane bending effect any further, as evidenced in Fig. 11(b). Instead, a steady decrease in the bending effect can be observed for the case $E_R/E_P = 3$, see Fig. 11(c). It should be noted, however, that the absolute values of the stress intensity factor would decrease quite significantly as the thickness ratio increases, as shown in Fig. 12, because the stiffness ratio S plays an important role in reducing the stress intensity factor for two-sided reinforcement. Figure

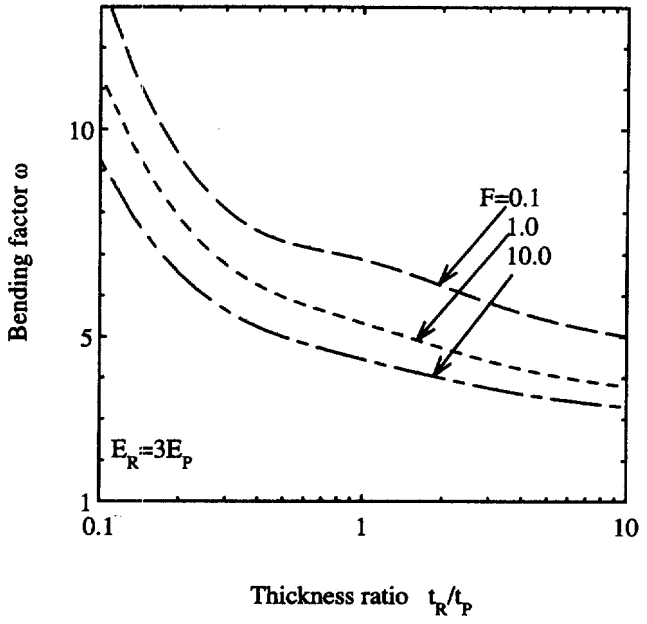

(c)

Fig. 11—*continued.*

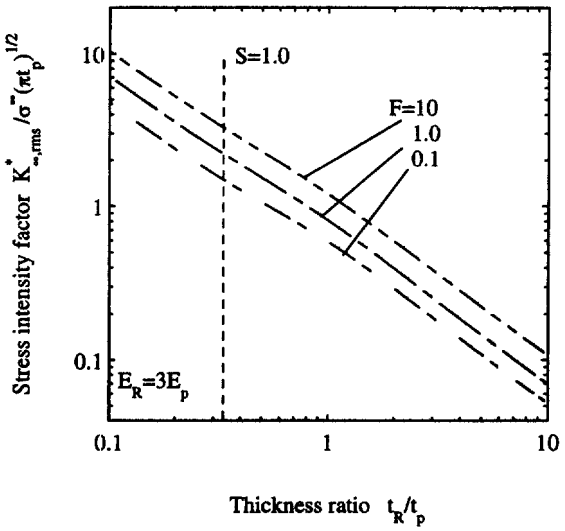

Fig. 12. Variation of the stress intensity factor for one-sided reinforcement with respect to thickness ratio.

12 clearly demonstrates the dramatic reduction in the stress intensity factor if thicker reinforcements are used. Therefore, it can be concluded that the most effective method in reducing the out-of-plane bending is to employ reinforcement of the maximum allowable thickness.

7. CONCLUSIONS

Based on the preceding theoretical and finite element studies, the following conclusions can be drawn from the present work:

(1) Due to the out-of-plane bending induced by load-path eccentricity, the stress distribution along the prospective crack path before the crack appears is higher than in the case of two-sided reinforcement.

(2) Localized bending of the reinforcement in an unsupported one-sided repair would induce a significant increase in the stress intensity factor, hence reducing the repair efficiency.
(3) The stress intensity factor (maximum, minimum or root-mean-square) approaches, but never exceeds, a limiting value with increasing crack length for the case of one-sided repair.
(4) An explicit analytical solution has been obtained for the asymptotic value of the root-mean-square of the stress intensity factor along the crack front. This estimate has been shown to agree well with finite element results and provide a conservative prediction suitable for design purposes.
(5) The variation of the stress intensity factor along the crack front is found to be approximately independent of the crack length, hence can be estimated based on the stress variation which would prevail in a patched, but uncracked, plate.
(6) Parametric studies have shown that the most effective method to reduce the out-of-plane bending effect is to employ thicker reinforcement.

REFERENCES

Arendt, C. and Sun, C. T. (1994) Bending effects of unsymmetric adhesively bonded composite repairs on cracked aluminium panels. *Proceedings of FAA/NASA International Symposium on Advanced Structural Integrity Methods for Airframe Durability and Damage Tolerance*, NASA Conference Publication 3274, Part 1, pp. 33–48.

Baker, A. A. and Jones, R. (ed.) (1988) *Bonded Repair of Aircraft Structures*. Martinus Nijhoff, New York.

Baker, A. A. (1993). Repair efficiency in fatigue-cracked aluminium components reinforced with boron/epoxy patches. *Fatigue Fracture in Engineering Material Structures* **16**(7), 753–765.

Benthem J. P. (1977) State of stress at the vertex of a quarter-infinite crack in a half-space. *International Journal of Solids and Structures* **13**, 479–492.

Gere, J. M. and Timoshenko, S. P. (1987) *Mechanics of Materials*, 3rd edn. Chapman and Hall, London.

Goland, M. and Reissner, E. (1944) The stresses in cemented joints. *Journal of Applied Mechanics* **11**, A17–A27.

Hartranft, R. J. and Sih, G. C. (1968) Effect of plate thickness on the bending stress distribution around through cracks. *Journal of Mathematics and Physics* **47**, 276–291.

Hart-Smith, L. J. (1982) Induced peel stresses in adhesively bonded joints. Douglas Aircraft Company, MDC J9422A.

Hui, C. Y. and Zehnder, A. T. (1993) A theory for the fracture of thin plates subjected to bending and twisting moments. *International Journal of Fracture* **61**, 211–229.

Jones, R. (1983) Neutral axis offset effects due to crack patching. *Composite Structures* **1**, 163–174.

Jones, R. (1988) Crack patching: design aspects. In *Bonded Repair of Aircraft Structures*, eds A. A. Baker and R. Jones, Martinus Nijhoff Publishers, New York, pp. 40–76.

Murakami, Y. (ed.) (1987) *Stress Intensity Factor Handbook*, Vol. 1. Pergamon Press, Oxford.

PAFEC Users' Manual (1995) PAFEC Limited. Strelley Hall, Nottingham, United Kingdom.

Ratwani, M. M. (1979) Cracked, adhesively bonded laminated structures. *AIAA Journal* **17**(9), 988–994.

Reissner, E. (1947) On bending of elastic plates. *Quarterly Journal of Applied Mathematics* **5**, 55–68.

Rose, L. R. F. (1981) An application of the inclusion analogy for bonded reinforcements. *International Journal of Solids and Structures* **17**, 827–838.

Rose, L. R. F. (1982) A cracked plate repaired by bonded reinforcements. *International Journal of Fracture* **18**(2), 135–144.

Rose, L. R. F. (1988) Theoretical analysis of crack patching. In *Bonded Repair of Aircraft Structures*, ed. A. A. Baker and R. Jones, Martinus Nijhoff, New York, pp. 77–105.

Rose, L. R. F., Callinan, R. J., Baker, A. A., Sanderson, S. and Wilson, E. S. (1995) Design validation for a bonded composite repair to the F-111 lower wing skin. *Proceedings of 2nd Pacific International Conference on Aerospace Science and Technology*, Vol. 1, pp. 333–336.

Sih, G. C. (1971) A review of the three-dimensional stress problem for a cracked plate. *International Journal of Fracture* **7**(1), 39–61.

Wang, C. H. and Rose, L. R. F. (1997a) Bonded repair of cracks under mixed mode loading. *International Journal of Solids and Structures*. In press.

Wang, C. H. and Rose, L. R. F. (1997b) On the design of bonded patches for one-sided repair. *Proceedings 11th International Conference on Composite Materials*, Gold Coast, Australia.

Wang, C. H. and Rose, L. R. F. (1997c) A crack bridging model one-sided bonded repairs. *International Journal of Fracture*. Submitted.

APPENDIX 1

Parametric study

For one-sided repair, the centroid of the composite section is:

$$\bar{z} = \frac{E_P t_P \bar{z}_P + E_R t_R \bar{z}_R}{E_P t_P + E_R t_R} = \frac{\bar{z}_P + S\bar{z}_R}{1+S} = t_P f_1(S, T), \tag{A1}$$

where

$$f_1(S,T)=\left(1+2S+S\frac{t_R}{t_P}\right)\Big/2(1+S). \tag{A2}$$

The moment of inertia for each individual layer is

$$I_P=t_P^3\left(\frac{1}{12}+\left(\frac{\bar{z}_P-\bar{z}}{t_P}\right)^2\right)=t_P^3\left(\frac{1}{12}+\frac{1}{4}\left(1-2\frac{\bar{z}}{t_P}\right)^2\right)$$

$$=t_P^3\left(\frac{1}{12}+\frac{1}{4}\left(1-\frac{1+2S+2t_R/t_P}{1+S}\right)^2\right), \tag{A3}$$

for the plate and

$$I_R=t_R^3\left(\frac{1}{12}+\frac{1}{4}\left(1-\frac{t_P+t_R/2-\bar{z}}{t_R}\right)^2\right)$$

$$=t_R^3\left(\frac{1}{12}+\frac{1}{4}\left(1-\frac{t_P}{t_R}-\frac{1}{2}+\frac{t_P}{t_R}\frac{1+2S+2t_R/t_P}{1+S}\right)^2\right)$$

$$=t_R^3\left(\frac{1}{12}+\frac{1}{4}\left(\frac{1}{2}-\frac{t_P}{t_R}+\frac{t_P}{t_R}\frac{1+2S+2t_R/t_P}{1+S}\right)^2\right), \tag{A4}$$

for the reinforcement. Let us define $T=t_R/t_P$. The moment of inertia of the composite section can be written as, noting $n=S/T$:

$$I_t=I_P+nI_R=t_P^3\left(I_P\left(S,\frac{t_R}{t_P}\right)+nI_R\left(S,\frac{t_R}{t_P}\right)\right)=t_P^3f_2(S,T), \tag{A5}$$

$$\frac{\beta}{\kappa}=\frac{\sqrt{\dfrac{\mu_A}{t_A}\left(\dfrac{1}{E'_Rt_R}+\dfrac{1}{E'_Pt_P}\right)}}{\sqrt[4]{\dfrac{E'_A}{4t_A}\left(\dfrac{12}{E'_Rt_R^3}+\dfrac{12}{E'_Pt_P^3}\right)}}=\left(\frac{(1+S)^2(1-\nu_A)}{6FS(1+T^2S)}\right)^{1/4}=f_3(F,S,T,\nu_A). \tag{A6}$$

Similarly the parameter Q can be expressed as:

$$Q=\frac{\beta}{\kappa(1+S)}\frac{1+3t_P/4t_R}{1+t_P/t_R}(1-TS)=Q(F,S,T,\nu_A). \tag{A7}$$

Therefore, the bending correction factor is a function of four independent parameters:

$$\omega=\omega(F,S,T,\nu_A). \tag{A8}$$